ISSN 0036-0244, Russian Journal of Physical Chemistry A, 2021, Vol. 95, No. 7, pp. 1418–1423. © Pleiades Publishing, Ltd., 2021.

PHYSICAL CHEMISTRY OF NANOCLUSTERS AND NANOMATERIALS

Fabrication and Luminescence Properties of $La_2O_2S:Tb^{3+}$ Hollow Nanofibers

Fei Bi[a,*], Jiaqi Li[b], Guangqing Gai[a], and Xiangting Dong[b,]**

[a] *Laboratory of Building Energy-Saving Technology Engineering, College of Material Science and Engineering, Jilin Jianzhu University, Changchun, 130118 China*

[b] *Key Laboratory of Applied Chemistry and Nanotechnology at Universities of Jilin Province, Changchun University of Science and Technology, Changchun, 130022 China*

**e-mail: bifei1224@163.com*

***e-mail: dongxiangting888@163.com*

Received May 2, 2020; revised May 2, 2020; accepted June 10, 2020

Abstract—$La_2O_2S:Tb^{3+}$ hollow nanofibers were successfully fabricated by sulfurization of the relevant $La_2O_3:Tb^{3+}$ hollow nanofibers via double-crucible method. The morphology and properties of the products were investigated in detail by X-ray diffraction (XRD), scanning electron microscopy (SEM) and fluorescence spectrometry. $La_2O_2S:Tb^{3+}$ hollow nanofibers were pure hexagonal phase with space group $P\bar{3}m1$ and were hollow-centered structure with the mean diameter of 160.03 ± 17.74 nm. Emission spectra indicate that $La_2O_2S:Tb^{3+}$ hollow nanofibers emit green light at 544 nm attributed to $^5D_4 \rightarrow {}^7F_5$ energy levels transition of Tb^{3+} ions. CIE analysis demonstrated that the light emitted by $La_2O_2S:Tb^{3+}$ hollow nanofibers corresponds to the green region, and color-tuned luminescence can be obtained by changing concentration of Tb^{3+} ions. The obtained material could be applied in the field of optical telecommunication and optoelectronic devices. The possible formation mechanism of $La_2O_2S:Tb^{3+}$ hollow nanofibers was also proposed.

Keywords: lanthanum oxysulfide, luminescence, hollow nanofibers, electrospinning

DOI: 10.1134/S0036024421070104

INTRODUCTION

Rare earth (RE) compounds were intensively used in high-performance luminescence and display devices, optic communication, energy storage, new energy resource etc., especial the RE as hosts. It is expected that smaller size phosphors can improve luminescent quantum efficiency (QE), and display resolution [1–3]. Thus, nanocrystals doped with RE ions have attracted a large amount of interest. In the earlier years, the photoluminescent properties of RE ions in zero-dimensional nanoparticles have been extensively investigated, including the local symmetry, electronic transition processes, surface effects etc. [4–6]. Moreover, in comparison with zero-dimensional nanoparticles, the shape anisotropy of one-dimensional structure provided a better model system to investigate the dependence of electronic transport, optical properties on size confinement and dimensionality. Among these one-dimensional nanomaterials, hollow nanofiber is a new kind of one-dimensional nanomaterials with special morphology. It has attracted increasing interest of scientists owing to its anisotropy, large length-to-diameter ratio, unique optical, electrical and magnetic performances [7–9]. Research on the fabrication and properties of hollow nanofibers has become one of the popular subjects of study in the realm of nanomaterials.

The lanthanide (La-Lu) oxysulfides are known as wide-gap (4.6–4.8 eV) materials suitable for activation with doping ions [10–13]. In addition, compared with the lanthanide oxides, oxysulfides are more efficient phosphors with a broader excitation band. Therefore, the lanthanide oxysulfides become a very important host of inorganic materials which have high potential for applications in various fields, such as color television picture tubes, radiographic imaging, field emission displays, and long-lasting phosphorescence. RE oxysulfides are more biocompatible than RE oxide, may be used as biological probes and labels. Some researchers have prepared the La_2O_2S nanocrystals by combustion and solid state methods [14–17].

In recent years, electrospinning technology has been extensively explored as a simple and versatile method for forming inorganic superfine nanofibers using polymer/inorganic composite as the precursor [18–20]. The morphology of materials can be con-

trolled by adjusting experimental conditions, such as the viscosity of spinning solution, relative air humidity, the structure of spinneret, spinning voltage, and the distance between the spinneret and the collector. Advantages of this novel process for fabricating 1D nanostructures include, but is not limited to, low cost, high efficiency and convenient assembly. It has been reported that the nanofibers were successfully synthesized *via* electrospinning [21–25].

In this study, pure hexagonal phase $La_2O_2S:Tb^{3+}$ hollow nanofibers were prepared through calcining the electrospun PVP/[$La(NO_3)_3$ + $Tb(NO_3)_3$] composite nanofibers, and then $La_2O_2S:x\%Tb^{3+}$ (x is the molar ratio of Tb^{3+} to (La^{3+} + Tb^{3+}), x = 1, 3, 5, and 7) hollow nanofibers were fabricated by sulfurization of $La_2O_3:x\%Tb^{3+}$ hollow nanofibers via a double-crucible method we newly proposed for the first time. The samples were systematically characterized, and a possible formation mechanism of $La_2O_2S:Tb^{3+}$ hollow nanofibers was also presented.

EXPERIMENTAL

Chemicals

Polyvinyl pyrrolidone (PVP) (K15, M_w = 10000, AR) was bought from Tiantai Chemical Co. Ltd. Yttrium oxide (La_2O_3, 99.99%) and terbium oxide (Tb_4O_7, 99.99%) were purchased from Kemiou Chemical Co., Ltd. *N*,*N*-dimethylformamide (DMF, AR) and Sulfur powder (S, AR) were purchased from Sinopharm Chemical Reagent Co. Ltd. Nitric acid (HNO_3, AR) was bought from Beijing Chemical Works. All chemicals were directly used as received without further purification.

Preparation of PVP/[$La(NO_3)_3$ + $Tb(NO_3)_3$] Composite Nanofibers via Electrospinning

In the typical procedure of preparing $La_2O_3:5\%Tb^{3+}$ hollow nanofibers, 1.14 g of La_2O_3 and 0.07 g of Tb_4O_7 were dissolved in dilute HNO_3 at elevated temperatures to form $RE(NO_3)_3{\cdot}6H_2O$ (RE = La^{3+} and Tb^{3+}). The rare earth nitrates were dissolved in 9.8 g of DMF, and then 7.8 g of PVP was added into the above solution. The solution was magnetically stirred for 10 h to form homogeneous transparent precursor solution. Subsequently, the precursor solution was electrospun at room temperature under a positive high voltage of 13 kV, the distance between the capillary tip and the collector (aluminium foil) was fixed to 16 cm, and relative humidity was 50–60%. PVP/[$La(NO_3)_3$ + $Tb(NO_3)_3$] composite nanofibers were obtained on the collector. Other series of $La_2O_3:x\%Tb^{3+}$ (x = 1, 3, and 7) hollow nanofibers were prepared by the similar procedure except for different doping molar concentration of Tb^{3+}.

Fabrication of $La_2O_3:Tb^{3+}$ Hollow Nanofibers

The above PVP/[$La(NO_3)_3$ + $Tb(NO_3)_3$] composite nanofibers were calcined at 700°C for 8 h with a heating rate of 1 K/min. Then the calcination temperature was decreased to 200°C at a rate of 1 K/min. Finally, samples were naturally cooled down to room temperature and $La_2O_3:Tb^{3+}$ hollow nanofibers were obtained.

Synthesis of $La_2O_2S:Tb^{3+}$ Hollow Nanofibers

$La_2O_3:Tb^{3+}$ hollow nanofibers were loaded into a small crucible. A few carbon rods were put into a big crucible, and then the small crucible was placed into the big crucible. Next, sulfur powder was loaded into the space between the two crucibles, and then the big crucible was covered with its lid. We call this process a double-crucible method. Finally the crucibles were heated at 800°C for 4 h under argon atmosphere, and then the temperature was decreased to 200°C at a rate of 1 K/min followed by natural cooling down to ambient temperature. Thus, $La_2O_2S:Tb^{3+}$ hollow nanofibers were obtained.

Characterization Methods

The X-ray diffraction (XRD) measurement was performed using a Rigaku D/max-RA XRD diffractometer with CuK_α radiation (0.15418 nm wavelength). The field emission scanning electron microscope (FESEM, XL-30, FEI Company) was used to characterize the morphologies and sizes of the products. The distribution histograms of diameters were plotted using Image-Pro Plus 6.0 and Origin 8.5 softwares. The excitation and emission spectra of samples were recorded with a HITACHI F-7000 fluorescence spectrophotometer using a Xe lamp as the excitation source.

RESULTS AND DISCUSSION

Crystal Structure

The XRD patterns of $La_2O_2S:Tb^{3+}$ hollow nanofibers are shown in Fig. 1. The XRD analysis of $La_2O_2S:Tb^{3+}$ hollow nanofibers demonstrates that the characteristic diffraction peaks of the samples can be easily indexed to those of the pure hexagonal phase with primitive structure of La_2O_2S (PDF no. 71-2098), and the space group is $P\bar{3}m1$. No peaks of any other phases or impurities are detected, indicating that crystalline $La_2O_2S:Tb^{3+}$ material was prepared via sulfurization of crystalline $La_2O_3:Tb^{3+}$.

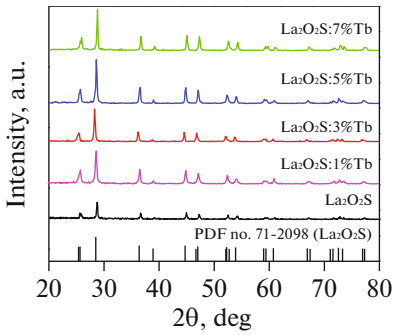

Fig. 1. XRD patterns of La_2O_2S:x%Tb^{3+} ($x = 0$, 1, 3, 5 and 7) hollow nanofibers.

Morphology

Figure 2 shows the representative SEM images of the PVP/[$La(NO_3)_3$ + $Tb(NO_3)_3$] composite nanofibers, La_2O_3:Tb^{3+} hollow nanofibers and La_2O_2S:Tb^{3+} hollow nanofibers. From the SEM image of Fig. 2a, it can be noticed that the PVP/[$La(NO_3)_3$ + $Tb(NO_3)_3$] composite nanofibers have uniform diameter with good dispersivity. Figure 2b shows the SEM image of as-prepared La_2O_3:Tb^{3+} hollow nanofibers. It can be clearly seen that the morphology of nanofibers is hollow-centered structure obtained by calcination of the respective electrospun PVP/[$La(NO_3)_3$ + $Tb(NO_3)_3$] composite nanofibers. After annealing and sulfurization at 800°C, as-formed La_2O_2S:Tb^{3+} hollow nanofibers have relatively smooth surface, as revealed in Fig. 2c. From Fig. 2c, one can see that the sample exhibits hollow-centered fibrous structure. It reveals that La_2O_2S:Tb^{3+} hollow nanofibers retain their 1D morphology. From above analyses, we can safely conclude that the sulfurization technique we proposed here can retain the morphology of the precursor nanofibers.

Under the 95% confidence level, the diameters of PVP/[$La(NO_3)_3$ + $Tb(NO_3)_3$] composite nanofibers, La_2O_3:Tb^{3+} hollow nanofibers and La_2O_2S:Tb^{3+} hollow nanofibers analyzed by Shapiro-Wilk method are normal distribution. Distribution histograms of diameters of the samples are indicated in Fig. 3. As seen from Fig. 3, the diameters of PVP/[$La(NO_3)_3$ + $Tb(NO_3)_3$] composite nanofibers, La_2O_3:Tb^{3+} hollow nanofibers and La_2O_2S:Tb^{3+} hollow nanofibers are 459.19 ± 52.62, 189.57 ± 22.69, and 160.03 ± 17.74 nm, respectively.

Photoluminescence Properties

Figure 4 shows the excitation (monitored by 544 nm) and emission (excited by 260 nm) spectra of La_2O_2S:x%Tb^{3+} ($x = 1$, 3, 5, and 7) hollow nanofibers. The excitation spectra (Fig. 4a) exhibits one strong broad band in the range from 200 to 300 nm with a maximum at 260 nm, which is attributed to transition of the electron from the ground state to the split 5*d* energy levels, namely $4f^8 \rightarrow 4f^7 5d^1$ energy levels transitions of Tb^{3+} [12, 15]. The emission spectra of La_2O_2S:x%Tb^{3+} ($x = 1$, 3, 5, and 7) hollow nanofibers is shown in the Fig. 4b. It is found from Fig. 4b that the green emission peaks consist of two main peaks at 489 and 544 nm, which originate from $^5D_4 \rightarrow {}^7F_J$ ($J = 6$ and 5) energy levels transitions of Tb^{3+} ions, respectively. The weak emission peak at 587 nm is ascribed to the $^5D_4 \rightarrow {}^7F_4$ energy level transitions of Tb^{3+} ions. Among these emission peaks, the green emission at 544 nm attributed to $^5D_4 \rightarrow {}^7F_5$ energy levels transition of Tb^{3+} ions is the strongest one.

Figure 4 demonstrates the PL spectra of La_2O_2S:Tb^{3+} hollow nanofibers with different concentrations of Tb^{3+} ions. It is found that the spectral shape and locations of excitation and emission peaks do not vary with the concentration of Tb^{3+} ions, but the intensity of excitation and emission peaks strongly depend on the concentration of Tb^{3+} ions. The strongest excitation and emission spectra can be obtained when the molar concentration of Tb^{3+} is 5%. Obviously, the luminescence intensity of La_2O_2S:Tb^{3+} hollow nanofibers increases with increase in the concentration of Tb^{3+} from the beginning, reaches a maxi-

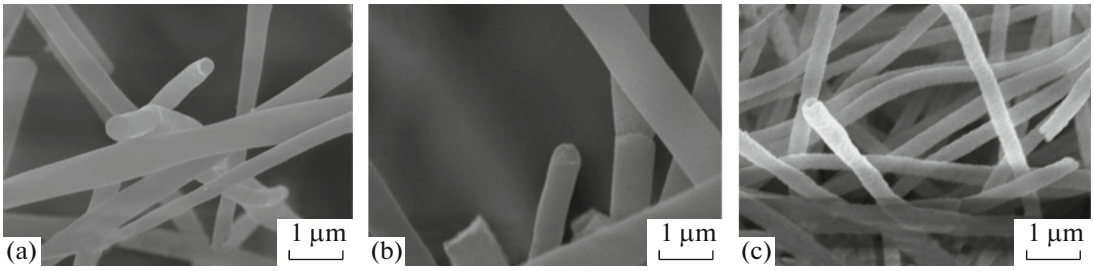

Fig. 2. SEM images of PVP/[$La(NO_3)_3$ + $Tb(NO_3)_3$] composite nanofibers (a), La_2O_3:Tb^{3+} hollow nanofibers (b), and La_2O_2S:Tb^{3+} hollow nanofibers (c).

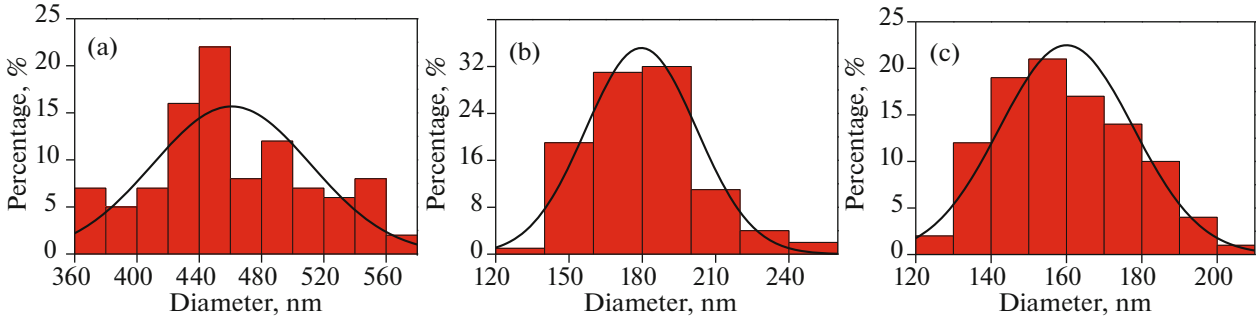

Fig. 3. Distribution histograms of diameters of PVP/[$La(NO_3)_3$ + $Tb(NO_3)_3$] composite nanofibers (a), La_2O_3:Tb^{3+} hollow nanofibers (b), and La_2O_2S:Tb^{3+} hollow nanofibers (c).

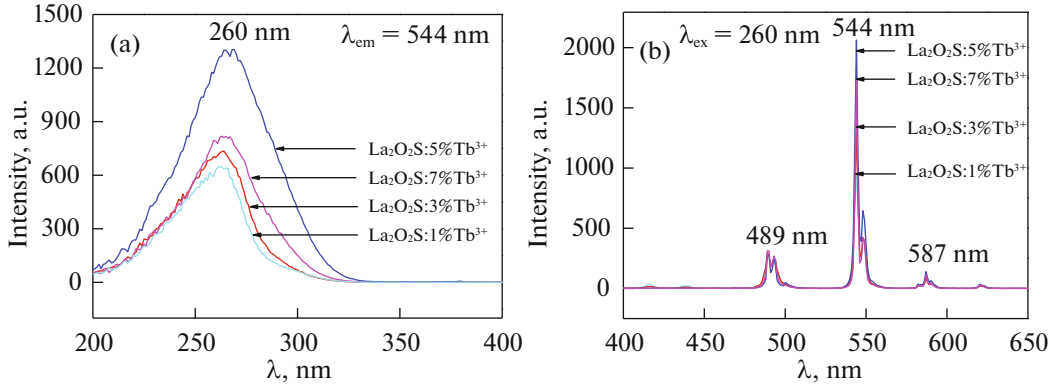

Fig. 4. Excitation (a) and emission (b) spectra of the La_2O_2S:x%Tb^{3+} (x = 1, 3, 5, and 7) hollow nanofibers.

mum value at Tb^{3+} concentration of 5%, and then decreases with further increase in Tb^{3+} concentration.

PL decay curves for La_2O_2S:x%Tb^{3+} (x = 1, 3, 5, and 7) hollow nanofibers with different concentrations of Tb^{3+} shown in Fig. 5, are used to calculate the lifetime and to investigate the luminescence dynamics of these samples. The luminescence was excited at 260 nm and monitored at 544 nm. It can be seen that all the curves can be well fitted with a single-exponential function as $I_t = I_0\exp(-t/\tau)$, where I_t is the intensity at time τ, I_0 is the intensity at $t = 0$, and τ is the decay lifetime. The fitting was performed using Origin 8.5 software, and the values of the parameter τ were obtained. The average luminescence lifetime for La_2O_2S:x%Tb^{3+} (x = 1, 3, 5, and 7) hollow nanofibers are 0.79, 0.89, 1.11, and 0.96 ms, corresponding to the Tb^{3+} concentration of 1, 3, 5, and 7%, respectively.

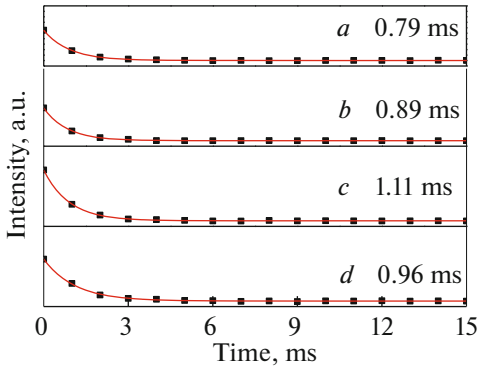

Fig. 5. Luminescence decay curves of La_2O_2S:x%Tb^{3+} (x = 1, 3, 5, and 7) hollow nanofibers.

CIE Analysis

Generally, color is represented by the Commission Internationale de L'Eclairage (CIE) chromaticity coordinates and color ratios. The chromaticity coordinates and color ratios have been calculated from the emission spectra by the method described in previous report [24]. For the La_2O_2S:x%Tb^{3+} (x = 1, 3, 5, and 7) hollow nanofibers, the chromaticity coordinates (X, Y) are determined to be (0.2520, 0.5749), (0.2573, 0.5977), (0.2646, 0.6109), and (0.2791, 0.6386), respectively. Remarkably, the change in emission color of La_2O_2S:x%Tb^{3+} (x = 1, 3, 5, and 7) hollow nanofibers with the variation of concentration of Tb^{3+} is shown in Fig. 6. These results indicate that the lumi-

nescence color can be tuned by changing the concentration of doping activator ions. The obtained nanostructures could be a promising material for LEDs.

Formation Mechanism for $La_2O_2S:Tb^{3+}$ Hollow Nanofibers

The formation mechanism for $La_2O_2S:Tb^{3+}$ hollow nanofibers is proposed on the basis of the above experimental results, as shown in Fig. 7. PVP, $La(NO_3)_3$ and $Tb(NO_3)_3$ were mixed with DMF to form precursor solution with certain viscosity. Then, PVP/[$La(NO_3)_3$ + $Tb(NO_3)_3$] composite nanofibers were obtained via electrospinning. During calcination process, PVP chain was broken and volatilize. The La^{3+}, Tb^{3+}, and NO_3^- ions moved to the surface of the composite fibers upon evaporation of solvent DMF. With the increase in calcination temperature, nitrates were decomposed to NO_2, La^{3+}, and Tb^{3+} and form $La_2O_3:Tb^{3+}$ crystallites. The crystallites were combined into nanoparticles, then some nanoparticles were mutually connected to generate hollow-centered $La_2O_3:Tb^{3+}$ nanofibers. PVP acted as template during the formation of $La_2O_3:Tb^{3+}$ hollow nanofibers. It was found from experiments that the average molecular weight of PVP and content of PVP in the precursor solution played important role in the formation of $La_2O_3:Tb^{3+}$ hollow nanofibers. Next, $La_2O_3:Tb^{3+}$ hollow nanofibers were sulfurized using sulfur powder. During the process, sulfur powder and $La_2O_3:Tb^{3+}$ hollow nanofibers were separated by the small crucible, which prevented $La_2O_3:Tb^{3+}$ hollow nanofibers from morphology damage. If $La_2O_3:Tb^{3+}$ hollow nanofibers were directly mixed with sulfur powder, molten sulfur destroyed $La_2O_3:Tb^{3+}$ hollow nanofibers. Carbon rods played an important role in the reduction via combination with O_2 to produce CO, which react with oxygen species of $La_2O_3:Tb^{3+}$ to give CO_2 in the heating process. The double-crucible

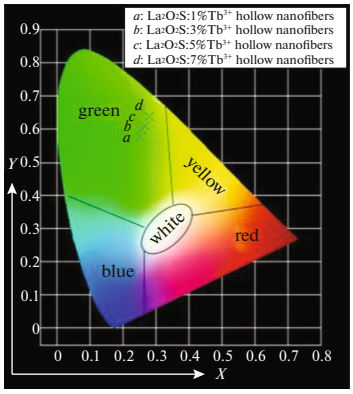

Fig. 6. CIE chromaticity coordinates diagram of $La_2O_2S:x\%Tb^{3+}$ (x = 1, 3, 5, and 7) hollow nanofibers.

method we proposed here is actually a solid–gas reaction, which has been proved to be an important method, not only can retain the morphology of $La_2O_3:Tb^{3+}$ hollow nanofibers, but also allows to fabricate single-phase $La_2O_2S:Tb^{3+}$ hollow nanofibers at relatively low temperature. Reaction scheme describing the formation of $La_2O_2S:Tb^{3+}$ hollow nanofibers can be written as follows:

$$\mathrm{PVP/[La(NO_3)_3 + Tb(NO_3)_3] + O_2} \xrightarrow{700^\circ\mathrm{C}} \mathrm{CO_2 + H_2O + NO_2 + La_2O_3:Tb^{3+}}, \quad (1)$$

$$\mathrm{C + O_2 \rightarrow CO}, \quad (2)$$

$$\mathrm{La_2O_3:Tb^{3+} + S + CO} \xrightarrow{800^\circ\mathrm{C}} \mathrm{La_2O_2S:Tb^{3+} + CO_2}. \quad (3)$$

CONCLUSIONS

In summary, pure hexagonal phase $La_2O_2S:Tb^{3+}$ hollow nanofibers with space group $P\bar{3}m1$ were fabricated via sulfurization of the $La_2O_3:Tb^{3+}$ hollow nano-

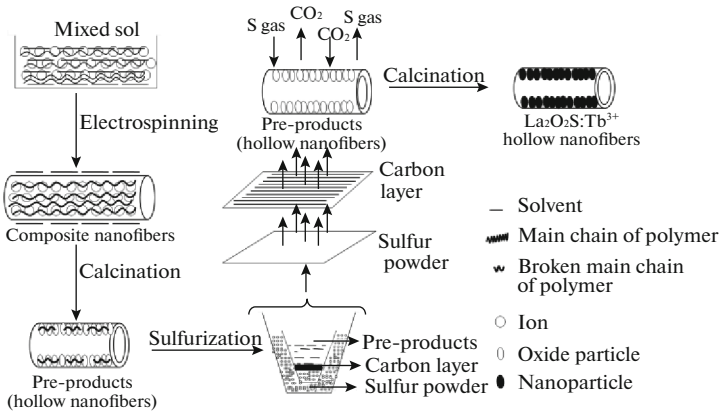

Fig. 7. Formation mechanism of $La_2O_2S:Tb^{3+}$ hollow nanofibers.

fibers. The morphology of the obtained nanofibers can be inherited from the precursor nanofibers under the sulfurization conditions via a double-crucible method we newly proposed. The diameter of $La_2O_2S:Tb^{3+}$ hollow nanofibers analyzed by Shapiro–Wilk method obeys normal distribution and is 160.03 ± 17.74 nm. Emission spectra show that $La_2O_2S:Tb^{3+}$ hollow nanofibers emit green light luminescence at 544 nm attributed to $^5D_4 \rightarrow {}^7F_5$ energy levels transition of Tb^{3+} ions. The double-crucible method we proposed here is of great importance. This technique can be employed in fabrication of other pure-phase rare earth oxysulfide nanomaterials with various morphologies.

ACKNOWLEDGMENTS

This work was financially supported by the National Natural Science Foundation of China (NSFC 50972020, 51072026), Ph.D. Programs Foundation of the Ministry of Education of China (20102216110002, 20112216120003), the Science and Technology Development Planning Project of Jilin Province (grant nos. 20070402, 20060504), Key Research Project of Science and Technology of Ministry of Education of China (grant no. 207026), the Science and Technology Research Project of the Education Department of Jilin Province during the thirteenth five-year plan period (grant nos. JJKH20180580KJ, JJKH20180582KJ) and the Scientific Development Program of Jilin Province (grant no. 20170520152JH).

REFERENCES

1. C. H. Yan, Z. Yan, Y. Du, J. Shen, C. Zhang, and W. Feng, in *Handbook on the Physics and Chemistry of Rare Earths* (Academic, Burlington, 2011), Vol. 41, p. 275.
2. D. G. Mancebo, A. I. Becerro, T. C. Rojas, A. Olivencia, A. Corral, M. Balcerzyk, E. Cantelar, F. Cussó, and M. Ocaña, J. Colloid Interface Sci. **520**, 134 (2018).
3. J. Shen, L. D. Sun, and C. H. Yan, Dalton Trans. **42**, 5687 (2008).
4. N. Shrivastava, U. Rocha, D. Muraca, W. Silva, C. Jacinto, R. Kumar, and S. K. Sharma, Mater. Lett. **213**, 358 (2018).
5. L. X. Lovisa, M. C. Oliveira, J. Andrés, L. Gracia, M. S. Li, E. Longo, R. L. Tranquilin, C. A. Paskocimas, M. R. D. Bomio, and F. V. Motta, J. Alloys Compd. **750**, 55 (2018).
6. Z. F. Li, T. Y. Yang, Q. Zhao, and M. Z. Zhang, Phys. Chem. Chem. Phys. **19**, 16758 (2017).
7. Y. W. Liu, Q. L. Ma, M. Yang, X. T. Dong, Y. Yang, J. X. Wang, W. S. Yu, and G. X. Liu, Chem. Eng. J. **284**, 831 (2016).
8. L. Han, Y. H. Hu, M. M. Pan, Y. F. Xie, Y. Y. Liu, D. Li, and X. T. Dong, CrystEngComm **17**, 2529 (2015).
9. J. D. Guo, Y. Yang, W. S. Yu, X. T. Dong, J. X. Wang, G. X. Liu, and T. T. Wang, RSC Adv. **6**, 111447 (2016).
10. G. D. Liu, Q. H. Zhang, H. Z. Wang, and Y. G. Li, Mater. Sci. Eng. B **177**, 316 (2012).
11. M. Pokhrel, A. K. Gangadharan, and D. K. Sardar, Mater. Lett. **99**, 86 (2013).
12. S. V. Yap, R. M. Ranson, W. M. Cranton, D. C. Koutsogeorgis, and G. B. Hix, J. Lumin. **129**, 416 (2009).
13. Y. M. Yang, C. Mi, F. Yu, X. Y. Su, C. F. Guo, G. Li, J. Zhang, L. L. Liu, Y. Z. Liu, and X. D. Li, Ceram. Int. **40**, 9875 (2014).
14. N. T. Lau, M. Fang, and C. K. Chan, Appl. Catal. B **79**, 110 (2008).
15. J. Bang, M. Abboudi, B. Abrams, and P. H. Holloway, J. Lumin. **106**, 177 (2004).
16. Y. Z. Huang, L. Chen, and L. M. Wu, Cryst. Growth Des. **8**, 739 (2008).
17. J. J. Oh, B. K. Jin, W. J. Chung, D. W. Shin, and Y. G. Choi, Curr. Appl. Phys. **11**, S15 (2011).
18. Y. T. Geng, P. Zhang, Q. T. Wang, Y. X. Liu, and K. Pan, J. Mater. Chem. B **5**, 5390 (2017).
19. C. Luo, X. X. Wang, J. Q. Wang, and K. Pan, Compos. Sci. Technol. **133**, 97 (2016).
20. N. Lv, J. L. Zhang, G. M. Li, X. Wang, and J. Z. Ni, J. Phys. Chem. C **121**, 11926 (2017).
21. N. Lv, Z. G. Wang, W. Z. Bi, G. M. Li, and J. L. Zhang, J. Mater. Chem. B **4**, 4402 (2016).
22. M. Gao, X. F. Lu, M. Q. Chi, S. H. Chen, and C. Wang, Inorg. Chem. Front. **4**, 1862 (2017).
23. M. Q. Chi, S. H. Chen, M. X. Zhong, C. Wang, and X. F. Lu, Chem. Commun. **54**, 5827 (2018).
24. L. B. Fan, Q. L. Ma, J. Tian, D. Li, X. Xi, X. T. Dong, W. S. Yu, J. X. Wang, and G. X. Liu, J. Mater. Sci. **53**, 2290 (2018).
25. J. Tian, Q. L. Ma, W. S. Yu, X. T. Dong, Y. Yang, B. Zhao, J. X. Wang, and G. X. Liu, N. J. Chem. **41**, 13983 (2017).